





Article

Hydrodynamic Loads in a Stilling Basin of a Converging Stepped Spillway: An Experimental Study

Bojan Milovanovic ¹, Predrag Vojt ², Budo Zindovic ^{1,*}, Vladan Kuzmanovic ¹ and Ljubodrag Savic ¹

¹ Chair of Hydraulic and Environmental Engineering, Faculty of Civil Engineering, University of Belgrade, 11000 Belgrade, Serbia; bmilovanovic@grf.bg.ac.rs (B.M.); vladak@grf.bg.ac.rs (V.K.); ljdsavic@grf.bg.ac.rs (L.S.)

² Institute for the Development of Water Resources “Jaroslav Cerni”, 11226 Belgrade, Serbia; predrag.vojt@jcerni.rs

* Correspondence: bzindovic@grf.bg.ac.rs

Abstract: This paper presents a methodology for estimation of hydrodynamic loads acting on the bottom and at the walls of a stilling basin of a stepped chute with converging walls, based on the pressure measurements at the selected points of a scale model. This is the first study of hydrodynamic loads for this type of structure, and the first one of the loads on the stilling basin walls in general. For selected flow discharges, step heights and hydraulic jump submergence ratio, the hydrodynamic pressures were measured at a significant number of points, providing the spatio-temporal distribution of relevant hydrodynamic loads. The most influential effect proved to be a convergence angle of the chute walls. Based on these measurements, appropriate regression expressions were proposed for predicting hydrodynamic loads. These expressions show good agreement with measurements, offering a reliable tool for the structural design of stepped spillway stilling basins.

Keywords: stilling basin; hydrodynamic load; stepped spillway; converging chute; pressure fluctuations



Citation: Milovanovic, B.; Vojt, P.; Zindovic, B.; Kuzmanovic, V.; Savic, L. Hydrodynamic Loads in a Stilling Basin of a Converging Stepped Spillway: An Experimental Study. *Water* **2024**, *16*, 140. <https://doi.org/10.3390/w16010140>

Academic Editor: Wencheng Guo

Received: 30 September 2023

Revised: 8 November 2023

Accepted: 15 November 2023

Published: 29 December 2023



Copyright: © 2023 by the authors. Licensee MDPI, Basel, Switzerland. This article is an open access article distributed under the terms and conditions of the Creative Commons Attribution (CC BY) license (<https://creativecommons.org/licenses/by/4.0/>).

1. Introduction

Stepped spillways have become common structures in large-dam hydraulic engineering due to the significant energy dissipation along the chute [1–7], hence considerably reducing the size and the cost of the stilling basin. The spillway crest should be wide enough to enable low overflow depth, enabling the minimum height of the dam, and the stilling basin should be narrow enough to minimize the excavation costs [8]. These two opposing conditions can be met only if the chute width narrows in the flow direction, i.e., using a chute with converging walls. Converging stepped spillways are an ongoing research topic, which has been investigated with scale and numerical models [8–11].

Pressure distribution at the contact of a fluid and solid boundary presents crucial data for the stilling basin structural design. Since they depend on a significant number of design and hydraulic parameters, pressures are often obtained from the scale-model measurements in a limited number of gauging points [12,13]. From measured values, engineers should devise a pressure distribution relevant for the structural design [14]. The transformation of pressure distribution to the design load (forces and bending moments) is a delicate task [15–17]. One alternative is to assume that the extreme pressures (minimum or maximum) extend over the entire slab/wall–water contact surface. This is extremely conservative, and results in extreme element dimensions, i.e., very thick slabs and/or walls. Alternatively, the cross-covariance matrix procedure, based on the fact that the extreme pressure cannot appear over the entire flow field in a single instant, could be used [18,19]. This procedure provides a more realistic estimate of the design load, but at the expense of the increased computational complexity, especially for a large number of gauging points and long sampling sequences. In order to completely preserve the nature of

the non-simultaneous occurrence of extreme pressures over the entire flow field, the procedure of direct statistical analysis (sorting of current values of total loads on the slab at the moment of sampling) for estimating the hydrodynamic loads was used in this research. Similar to [11], it is assumed that the probability density function of the sampled data can be well approximated by normal distribution.

Dynamic load for stilling basins has been the subject of research for smooth converging chutes [9] and in plunge pools with hydraulic jump [11,20]. Although there is some amount of experimental research on the stepped stilling basin flow in general [4,21,22], there are few published reports on the subject of dynamic loads in the stepped chute stilling basins [6], and, to the authors' knowledge, there is currently no published research in the area of dynamic loads in the basins of stepped chutes with variable bottom width (chutes with converging walls). In addition, there are no studies on the load on the stilling basin walls in the available literature.

The aim of this research is to present the pressure distributions obtained from the measurements in a stilling basin of a converging-walls stepped spillway scale model and to provide regression expressions for reliable estimation of design loads at the bottom and on the walls of such structures.

2. Methodology

2.1. Hydrodynamic Load Characterization

At any point in the flow field, instantaneous pressure, p , can be decomposed into mean pressure, \bar{p} , and pressure fluctuation, p' :

$$p = \bar{p} + p'. \quad (1)$$

Mean pressure is defined as a time-averaged integral:

$$\bar{p} = \frac{1}{T} \int_0^T p \cdot dt, \quad (2)$$

with T being the total measurement time [18], while pressure fluctuation can be estimated through standard deviation:

$$\sigma = \sqrt{p'^2} = \sqrt{\frac{1}{T} \int_0^T (p - \bar{p})^2 \cdot dt}. \quad (3)$$

The design load on the stilling-basin horizontal bottom slab is a vertical component of the hydrodynamic force. As well as pressures, the hydrodynamic force can be decomposed into time-averaged force (mean force), \bar{V} , and fluctuating component, V' :

$$V = \int_A p \cdot n \cdot dA = \int_A \bar{p} \cdot n \cdot dA + \int_A p' \cdot n \cdot dA = \bar{V} + V', \quad (4)$$

where n is the outward-pointing unit normal (the cosine of the angle between the normal of the surface and the direction of the load), while A is the area of the surface. To design the vertical wall of the basin, it is necessary to determine the hydrodynamic shear force, H , and bending moment, M . The loads on the wall per unit length can be decomposed as:

$$H = \int_0^{h_3} p(z) \cdot dz = \int_0^{h_3} \bar{p}(z) \cdot dz + \int_0^{h_3} p'(z) \cdot dz = \bar{H} + H', \quad (5)$$

$$M = \int_0^{h_3} p(z) \cdot z \cdot dz = \int_0^{h_3} \bar{p}(z) \cdot z \cdot dz + \int_0^{h_3} p'(z) \cdot z \cdot dz = \bar{M} + M', \quad (6)$$

where h_3 is the flow depth at a given point along the wall.

2.2. Dimensional Analysis

To estimate the values of design loads (forces and moment), one needs to understand the characteristics of the flow in the stilling basin. The flow field in a stepped-spillway stilling basin can be described with a large number of variables. These include geometric characteristics, flow conditions and physical properties of fluid. Geometric conditions are related to the spillway step height, s , and convergence angle of the chute walls, θ , (Figure 1).

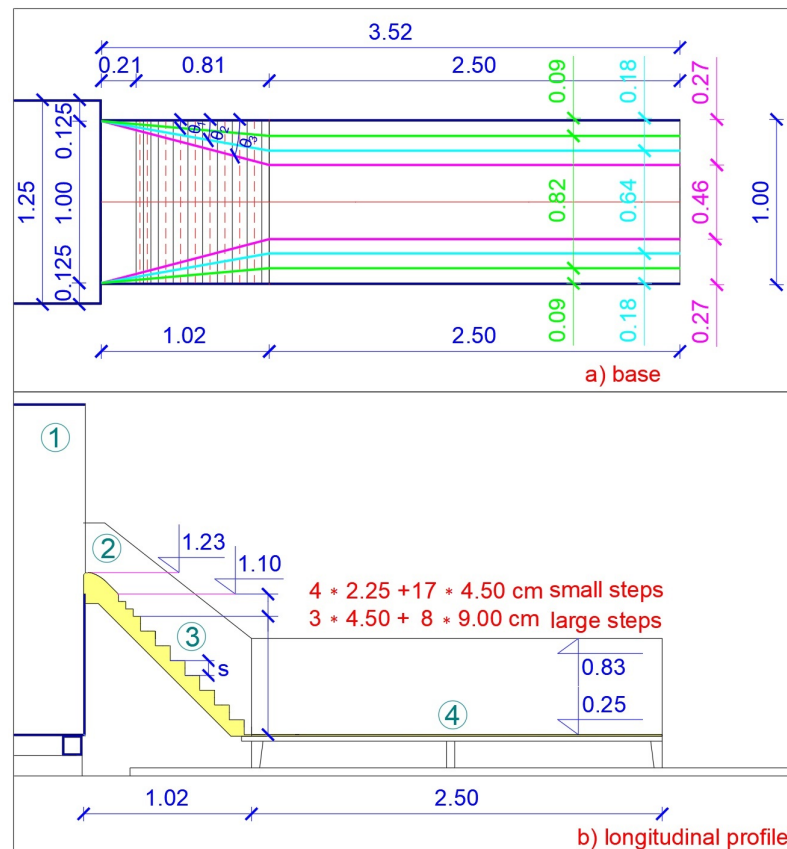


Figure 1. Geometric conditions: spillway step height, s , and convergence angle of the chute walls, θ . Parts of the model include: 1—reservoir, 2—weir, 3—stepped spillway, 4—stilling basin.

Flow conditions are related to inflow depth and velocity, h_1 and v_1 , and tail-water depth, h_{tw} (Figure 2). Physical characteristics of fluid include density, ρ_w , dynamic viscosity, μ_w , bulk modulus, E_w , and surface tension between water and air, τ_w . As the gravitational effects are important in open-channel flow, gravity, g , is included also. Taking all these variables into account, one can deduce the general form of the equation describing an arbitrary flow variable, Y :

$$Y = f(s, \theta, h_1, v_1, h_{tw}, \rho_w, \mu_w, E_w, \tau_w, g), \tag{7}$$

or in non-dimensional form:

$$Y^* = f(\chi, \theta, \Omega, Re_1, Ca_1, We_1, Fr_1), \tag{8}$$

where $\chi = \frac{s}{h_1}$ is a relative step height, $\Omega = \frac{h_{tw}}{h_2}$ is the hydraulic jump submergence ratio, h_2 is a second conjugate depth and Re_1 , Ca_1 , We_1 and Fr_1 are Reynolds, Cauchy, Weber and Froude numbers at the inflow section (the upstream end of the basin, i.e., the downstream end of the chute), respectively.

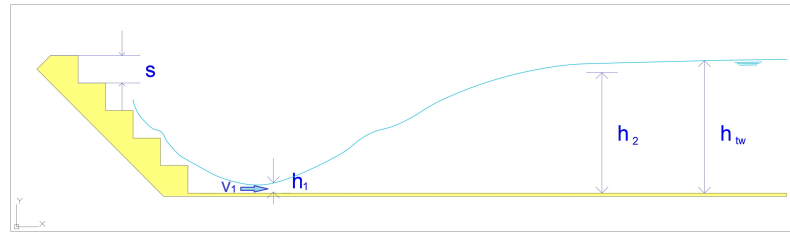


Figure 2. Flow conditions: inflow depth, h_1 , inflow velocity, v_1 , and tail-water depth, h_{tw} .

For the flow field in the stilling basin, close to the solid boundaries, the influence of Re_1 , Ca_1 and We_1 can be neglected [23], and the resulting form of the equation becomes:

$$Y^* = f(\chi, \theta, Fr_1, \Omega). \quad (9)$$

The first three terms in Equation (9) define upstream conditions for the stilling basin (i.e., the downstream end of the converging stepped chute), while the last term presents the tail-water effects.

2.3. Scale Models

Pressure measurements in the stepped-spillway stilling basin were performed on a modular scale model (Figure 3) that was used in previous research related to the stepped spillways and stilling basins [4,8,24]. The model was designed to accommodate variations in parameters outlined in Equation (9). Variable geometric parameters included a variation of a step height and a convergence angle of a stepped chute (Figure 1). The model was designed for a maximum flow rate of $Q = 100 \frac{L}{s}$.



Figure 3. Scale model of converging stepped chute with stilling basin.

The stepped spillway used in this study was designed for two different step heights (Figure 1b):

1. small steps ($s = 4.5$ cm), labelled as “S”,
2. large steps ($s = 9$ cm), labelled as “L”,

and four different convergence angles (i.e., four different widths, Figure 1a):

1. no convergence $\theta = 0^\circ$ ($B = 100$ cm), labelled as “0”,
2. small convergence angle $\theta = 5.5^\circ$ ($B = 80$ cm), labelled as “1”,
3. medium convergence angle $\theta = 11^\circ$ ($B = 60$ cm), labelled as “2”,

4. large convergence angle $\theta = 16.5^\circ$ ($B = 40$) cm, labelled as “3”, where B is the chute width at the downstream end and, in turn, the width of a stilling basin. Unlike the converging chute walls of the stepped spillway, the walls of the stilling basin were parallel (i.e., the basin was prismatic). The stilling basin was placed in the upstream reach of a 250 cm long prismatic rectangular canal. The length of the basin varied with the flow rate and was selected to be five sequent depths. This is in agreement with the general recommendations for the stilling basin’s design [3,25]. The downstream part of the canal had devices for adjusting the water level.

The range of Froude numbers in this research was between 20 and 70, the range of relative step height was between 0.1 and 0.3, the range of convergence angles was between 0 and 16.5 and the range of submergence was between 1 and 1.25.

2.4. Measurements

Locations of pressure gauges used in this study are presented in Figures 4 and 5. The number of measurement locations placed on the bottom varied between 9 for the narrowest variant and 24 for the widest to accommodate for different widths of the stilling basins (Figure 4). Pressure on the wall was measured in six cross-sections at two levels per section (Figure 5).

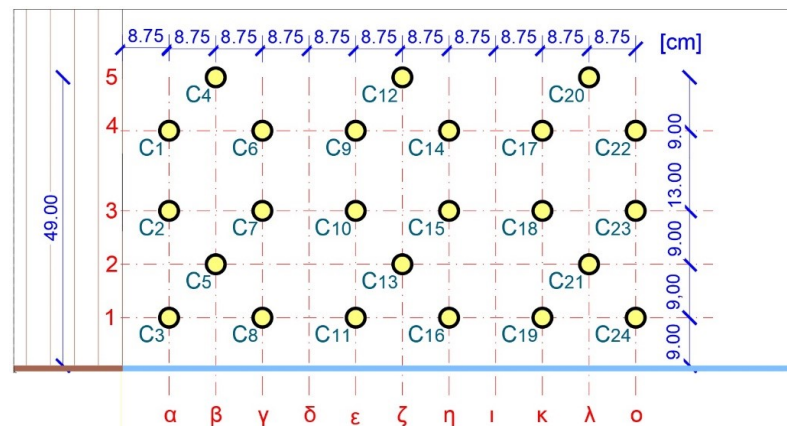


Figure 4. Locations of pressure gauges at the bottom.

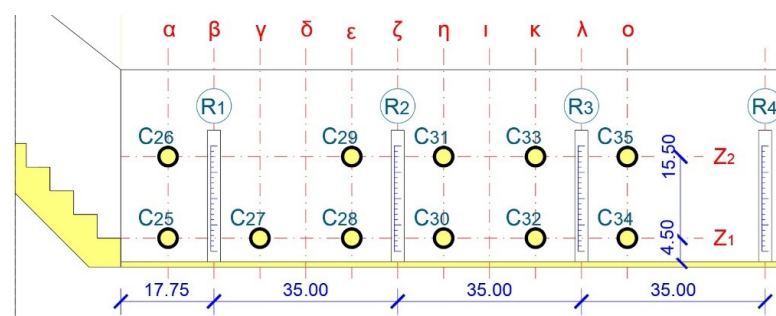


Figure 5. Locations of pressure gauges on the wall.

Pressure was measured for every chute wall-convergence angle (labelled as 0, 1, 2 and 3) for small and large steps (labelled as S and L). The flow rate was varied between 20 and $60 \frac{L}{s}$. In addition, experiments included the variable tail-water depth, i.e., hydraulic jump submergence ratio, Ω .

Pressure was measured with DRUCK pressure gauges, with 0.1% accuracy. During the preliminary experiments, the authors examined the influence of sampling duration on the statistical parameters of the pressure distribution and concluded that a sampling length of 120 s with a sampling rate of 200 Hz was sufficient to obtain stable statistics. For synchronous data acquisition, we used “HBM QuantumX”.

Velocities and depths at the downstream end of the stepped spillway (i.e., at the upstream end of the stilling basin) were obtained from a previous study [8], where the used measurement technique and measurement methodology were presented in detail.

3. Results and Discussion

Mean pressures and pressure fluctuations were measured at the selected points on the walls and the bottom of the stilling basin (Figures 4 and 5) for the selected converging angles, θ , and step heights, s , and varying Froude number, Fr_1 , and tailwater levels (i.e., submergence ratios, Ω). The measured values were statistically processed and presented as a dimensionless ratio of the measured pressure (i.e., the height of a water column) and the incoming-flow specific energy (specific energy at the entry section of the stilling basin). In order to examine the dependence of the pressure on the parameters determined by dimensional analysis, the value of one of the parameters was varied while the others were kept constant.

3.1. Pressure Distribution at the Bottom

The bottom of the stilling basin consists of one or more horizontal slabs. Considering the inherent instability of the inflow jet, it is hydraulically advantageous for the slab to be as long as possible, as this reduces the risk of simultaneous occurrence of extreme pulsation pressures along the entire slab [3], thus reducing the total vertical force. On the other hand, a slab that is too long is susceptible to cracking due to thermal stresses; hence, for long stilling basins, it is necessary to divide the structure into two or more slabs along the length of the basin. In this study, two options were considered: (a) there is only one slab, and (b) the basin is divided lengthwise into two equal slabs. Values on the abscissa are presented in Figure 4 with axis “0” located at the toe of the right wall of the stilling basin.

Although it was found that pressure distributions for the steps do not fit normal distribution [26], results show that pressure distributions for the stilling basin can be well approximated with a normal distribution for every measurement location (Figure 6). This finding is similar to [11] for smooth spillway basins, although the discrepancy is less pronounced for stepped-chute spillways. This result shows that the pressure distribution for the steps and the basin differs, which might be caused by the intense turbulent mixing inside the hydraulic jump in the basin itself.

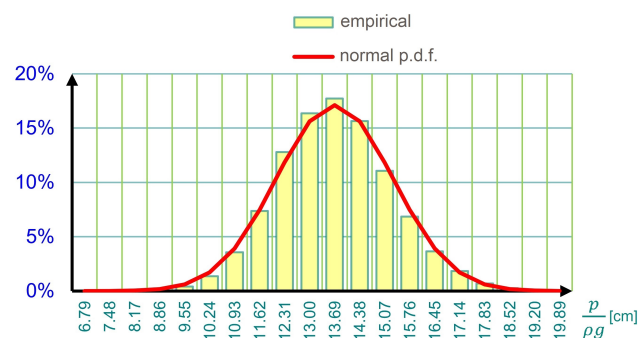


Figure 6. Comparison of a typical empirical (labelled *empirical*) and the normal probability density function (labelled *normal p.d.f.*) for the pressure head. Values on the abscissa are mid-points of bins of the histogram.

The research results indicate that the pressure distribution on the bottom is more pronounced than that on the walls. Figure 7 shows the variation in mean pressures when the inflow Froude number changes. Figure 8 shows the corresponding variation in the distribution of pressure fluctuations. It can be concluded that pressure fluctuations are significantly more pronounced in the upstream part of the stilling basin, where they reach up to 25% of the corresponding mean pressures. However, this occurs in small zones and should be taken into account only if the basin is designed with a large number of small slabs.

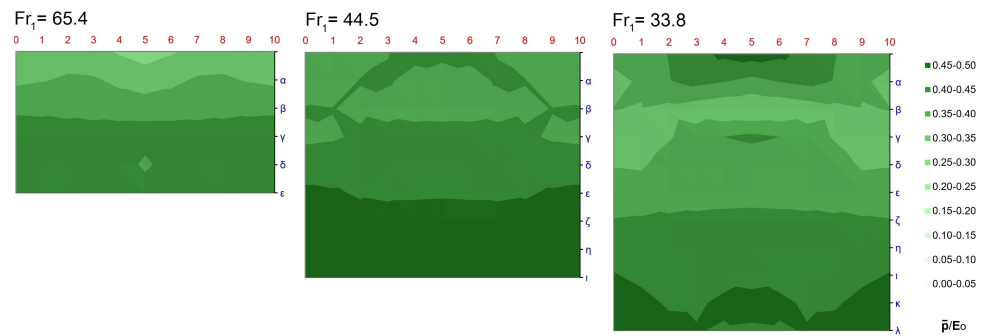


Figure 7. The influence of the Froude number, Fr_1 , on the mean pressures, \bar{p}/E_0 , at the bottom for $\theta = 0^\circ$, $\chi \approx 0.25$ and $\Omega \approx 1.15$ (dimensionless pressure fluctuations, expressed through standard deviation, $\frac{\sigma}{E_0}$).

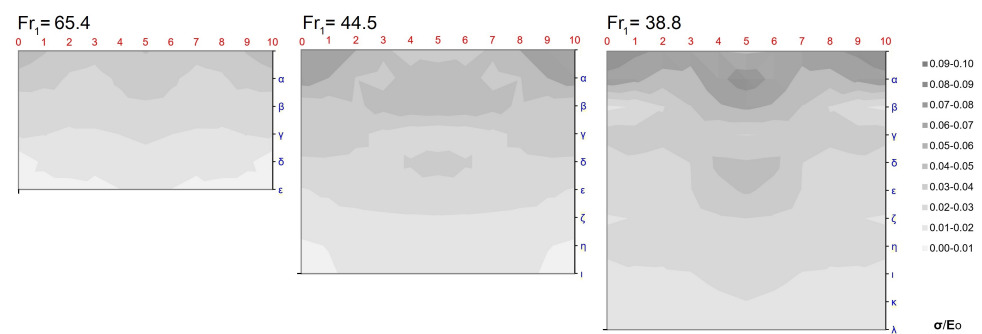


Figure 8. The influence of the Froude number, Fr_1 , on the pressure fluctuations, $\frac{\sigma}{E_0}$, at the bottom for $\theta = 0^\circ$, $\chi \approx 0.25$ and $\Omega \approx 1.15$.

The influence of the stepped-chute convergence angle on the pressure distribution at the bottom is presented in Figures 9 and 10. Figure 10 shows that with the increase in the angle, the pressure fluctuations on the bottom increase in the upstream regions of the basin and can be up to three times larger than in the case of a standard spillway chute (wall angle 0°). This can be attributed to the flow separation caused by the converging chute walls. Variation in chute convergence angle causes significantly greater changes in the vertical force, both on the entire basin and on its upstream and downstream parts, compared to the corresponding changes due to the variation of the Froude number.

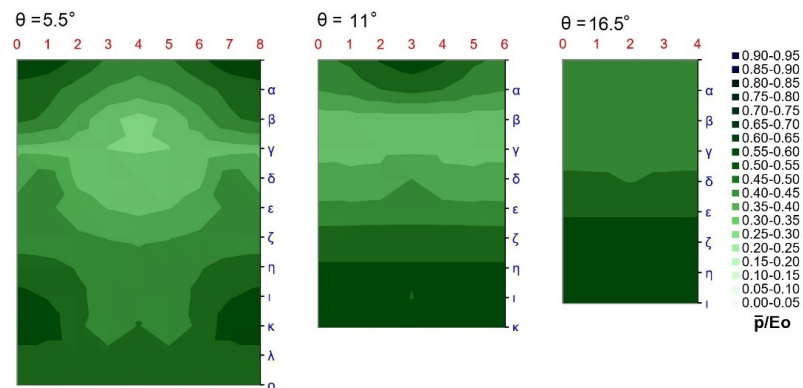


Figure 9. The influence of the convergence angle, θ , on the mean pressures, \bar{p}/E_0 , at the bottom for the Froude number $Fr_1 = 30$, large step $\chi \approx 0.25$ and submergence ratio $\Omega \approx 1.10$.

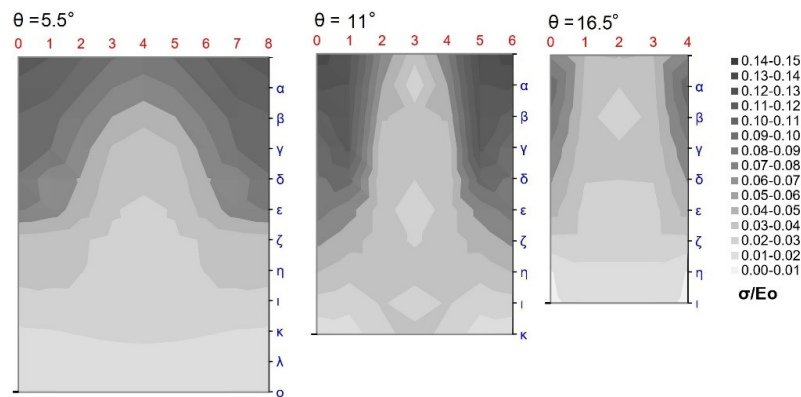


Figure 10. The influence of the convergence angle, θ , on the pressure fluctuations, $\frac{\sigma}{E_0}$, at the bottom for the Froude number $Fr_1 = 30$, large step $\chi \approx 0.25$ and submergence ratio $\Omega \approx 1.10$.

The influence of tail-water depth on pressure distribution is presented in Figures 11 and 12. Figure 11 shows that the increase in tail-water depth increases the mean pressure in the basin. This increase is proportional to the hydraulic jump submergence ratio for downstream regions, while in the upstream region it goes up to 1.5 of the submergence ratio. For pressure fluctuations (Figure 12), change in tail-water depth has a strong influence on spanwise distribution in the regions close to the upstream section, while in the downstream region of the basin its effect is negligible.

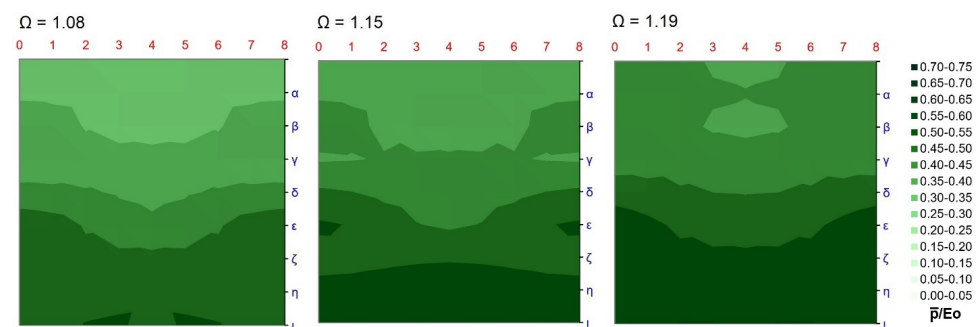


Figure 11. The influence of the submergence ratio, Ω , on the mean pressures, $\frac{\bar{p}}{E_0}$, at the bottom for the Froude number $Fr_1 = 33$, small step $\chi \approx 0.13$ and convergence angle $\theta = 5.5^\circ$.

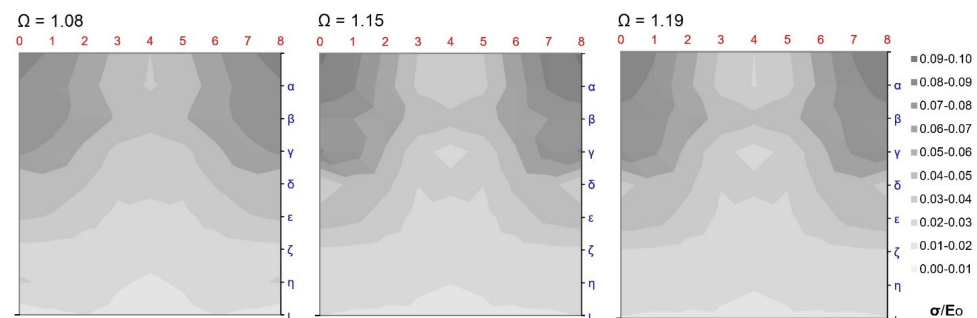


Figure 12. The influence of the submergence ratio, Ω , on the pressure fluctuations, $\frac{\sigma}{E_0}$, at the bottom for the Froude number $Fr_1 = 33$, small step $\chi \approx 0.13$ and convergence angle $\theta = 5.5^\circ$.

Figures 13 and 14 present the influence of the chute step size on the pressure distribution at the bottom of the basin. Large steps (larger chute roughness) produce higher energy dissipation compared to small steps, creating a larger depth of water and an increase in pressure fluctuations in the upstream region. The increase in fluctuations is possibly caused by larger local jumps and splashes over the larger steps.

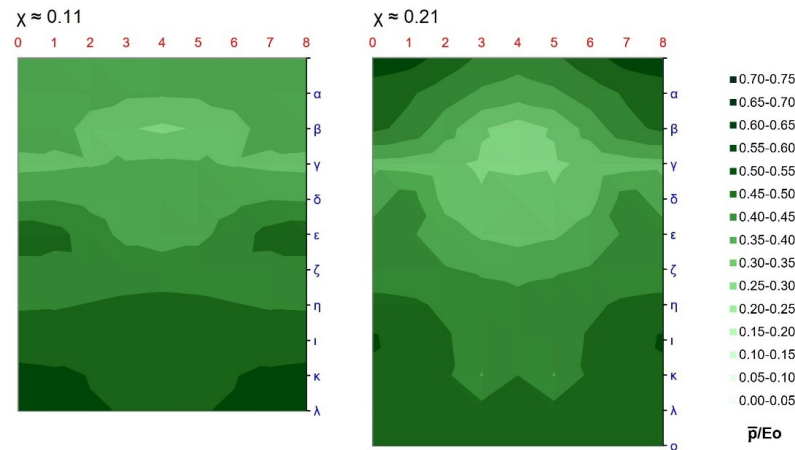


Figure 13. The influence of the chute step size, χ , on the mean pressures, $\frac{\bar{p}}{E_0}$, at the bottom for the Froude number $Fr_1 = 30$, submergence ratio $\Omega = 1.04$ and convergence angle $\theta = 5.5^\circ$.

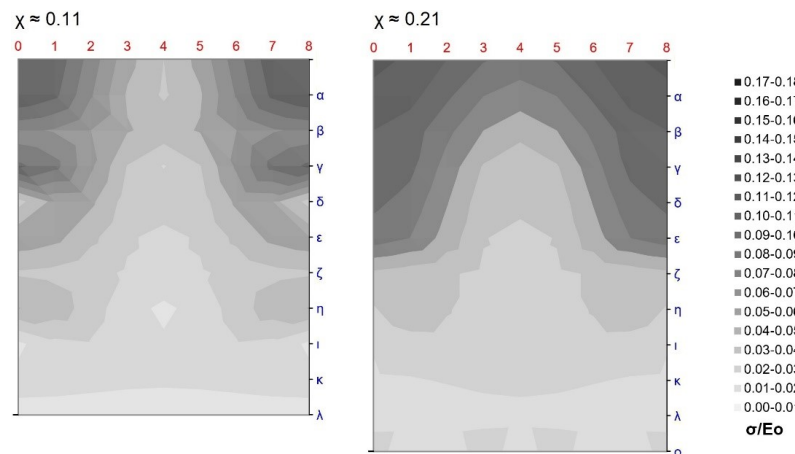


Figure 14. The influence of the chute step size, χ , on the pressure fluctuations, $\frac{\sigma}{E_0}$, at the bottom for the Froude number $Fr_1 = 30$, submergence ratio $\Omega = 1.04$ and convergence angle $\theta = 5.5^\circ$.

3.2. Pressure Distribution on the Wall

The influence of the incoming-flow Froude number, Fr_1 , on the pressure distribution along the wall for convergence angle $\theta = 0^\circ$, large steps $\chi \approx 0.25$ and submergence $\Omega \approx 1.15$ is presented in Figure 15 (dimensionless mean pressures, $\frac{\bar{p}}{E_0}$) and Figure 16 (dimensionless pressure fluctuations, expressed through standard deviation, $\frac{\sigma}{E_0}$), where $E_0 = h_0 + \frac{V_0^2}{2g}$ is specific energy at the beginning of the stilling basin. Values on abscissa are non-dimensional depths, i.e., vertical distance divided with twice the value of tail-water depth. Values on the ordinate axis represent the position of the cross-section in the flow direction, presented in Figure 5. All the measurements were taken along the reach of the basin where the hydraulic jump is formed (approximately five times the length of the sequent depth of the jump).

It can be observed from Figure 15 that the largest mean pressures on the wall occur in the downstream region of the stilling basin, where the load varies weakly with the change in Froude number. It should be noted that for the entire wall, the relevant section is the one where the greatest loads occur, hence the change of load along the basin does not affect the dimensions of the wall.

On the other hand, Figure 16 shows that the strongest pressure fluctuations are exhibited within the upstream region of the wall. This behavior can be attributed to the strong turbulence intensity of the incoming jet. The downstream regions of the basin wall showed the lowest values in pressure fluctuations, which can be attributed to the decrease

in turbulence intensity caused by the decrease in flow velocity. By comparing the mean values and standard deviations of the pressure distribution, one can conclude that the pressure fluctuations in the upstream regions of the wall amount to 20% to 30% of the mean pressure, with insignificant influence of the Froude number. For the downstream part, pressure fluctuations are significantly smaller, being roughly 2% of the mean pressure.

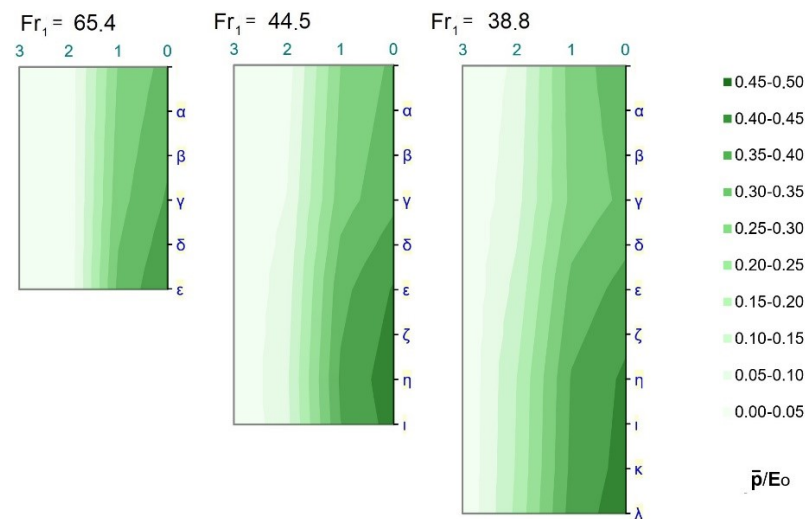


Figure 15. The influence of the Froude number, Fr_1 , on the mean pressures, $\frac{\bar{p}}{E_0}$, along the wall for $\theta = 0^\circ$, $\chi \approx 0.25$ and $\Omega \approx 1.15$ (dimensionless pressure fluctuations, expressed through standard deviation, $\frac{\sigma}{E_0}$).

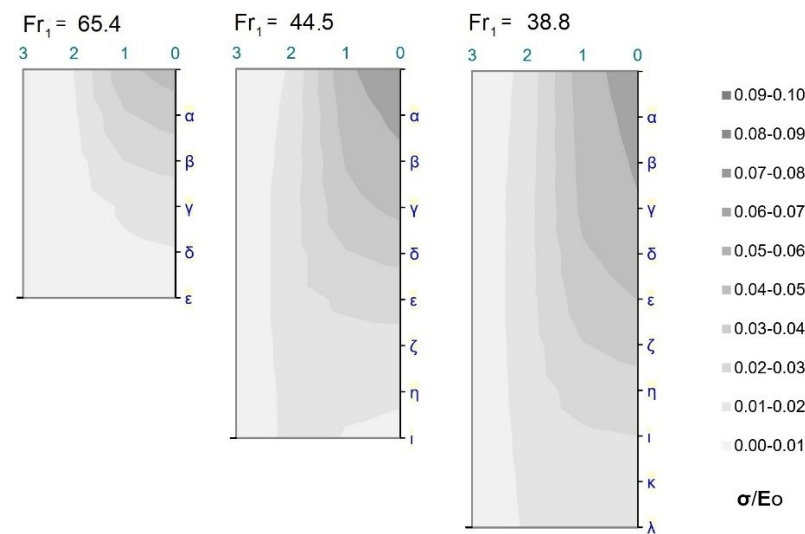


Figure 16. The influence of the Froude number, Fr_1 , on the pressure fluctuations, $\frac{\sigma}{E_0}$, along the wall for $\theta = 0^\circ$, $\chi \approx 0.25$ and $\Omega \approx 1.15$.

The influence of the convergence angle, θ , on the mean pressure distribution along the wall for Froude number $Fr_1 = 30$, large step $\chi \approx 0.25$ and submergence ratio $\Omega \approx 1.10$ is presented in Figure 17. Increasing the chute convergence angle slightly alters the distribution of mean pressures in the downstream end of the basin, yet with little significance for the wall design.

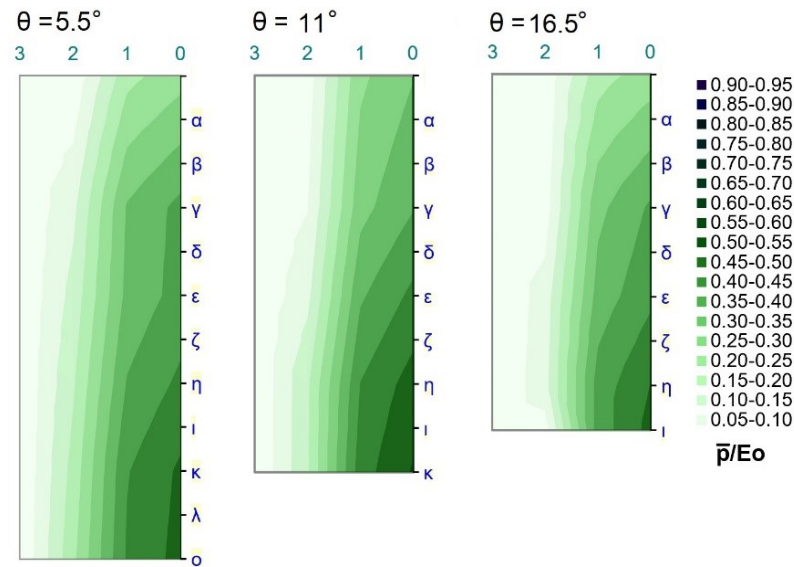


Figure 17. The influence of the convergence angle, θ , on the mean pressures, $\frac{\bar{p}}{E_0}$, along the wall for the Froude number $Fr_1 = 30$, large step $\chi \approx 0.25$ and submergence ratio $\Omega \approx 1.10$.

The influence of the convergence angle, θ , on the pressure fluctuations distribution along the wall for the Froude number $Fr_1 = 30$, large step $\chi \approx 0.25$ and submergence ratio $\Omega \approx 1.10$ is presented in Figure 18. The pressure fluctuations decrease slightly with the increase in the convergence of the supercritical flow, primarily within the most upstream region of the basin. At the most downstream section, fluctuations are almost negligible compared to the mean pressures.

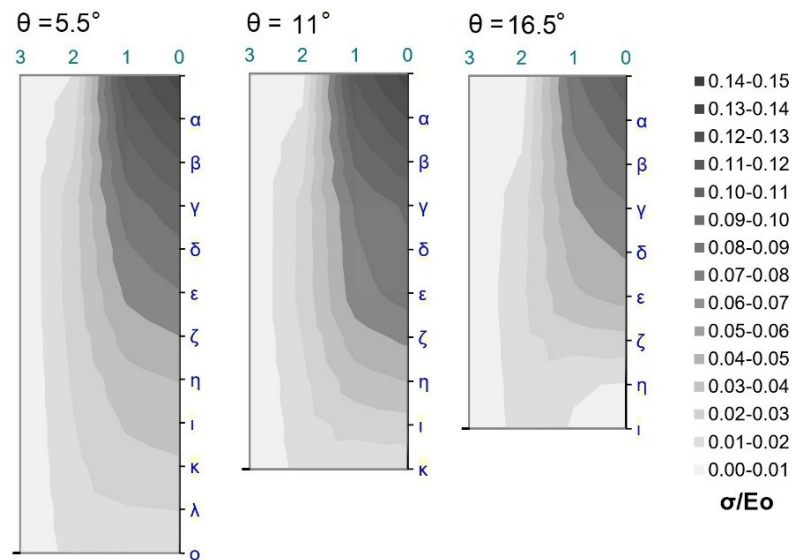


Figure 18. The influence of the convergence angle, θ , on the pressure fluctuations, $\frac{\sigma}{E_0}$, along the wall for the Froude number $Fr_1 = 30$, large step $\chi \approx 0.25$ and submergence ratio $\Omega \approx 1.10$.

The influence of the submergence ratio, Ω , on the pressure distribution along the wall for the Froude number $Fr_1 = 33$, small step $\chi \approx 0.13$ and convergence angle $\theta = 5.5^\circ$ is presented in Figures 19 and 20. Mean pressures increase slightly with increasing submergence, while the influence on the pressure fluctuations is negligible, except in the most upstream zone of the jump.

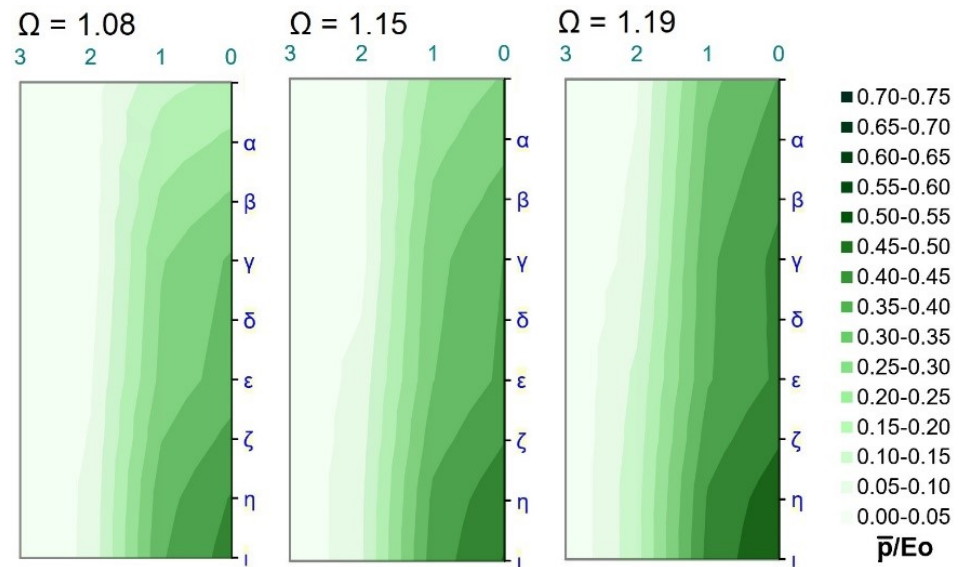


Figure 19. The influence of the submergence ratio, Ω , on the mean pressures, $\frac{\bar{p}}{E_0}$, along the wall for the Froude number $Fr_1 = 33$, small step $\chi \approx 0.13$ and convergence angle $\theta = 5.5^\circ$.

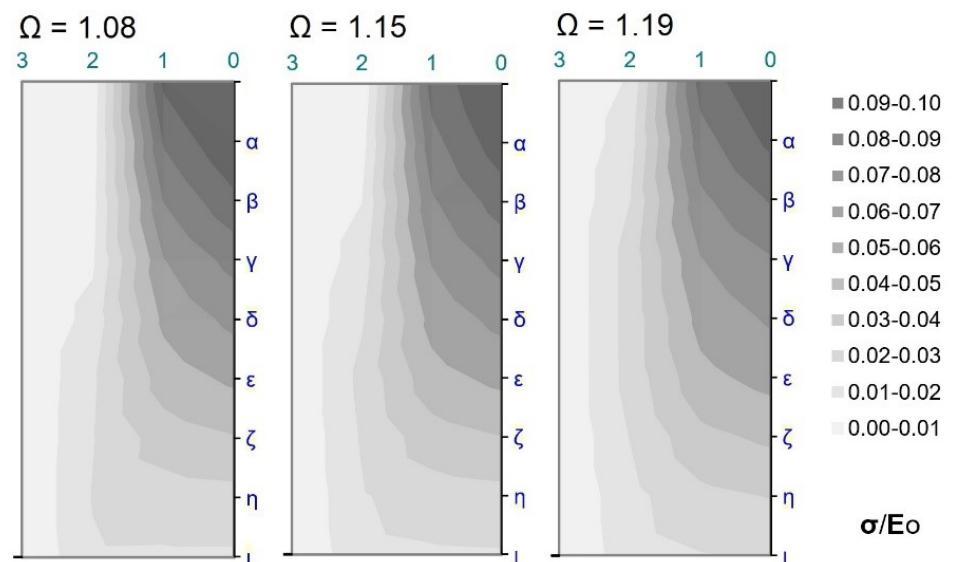


Figure 20. The influence of the submergence ratio, Ω , on the pressure fluctuations, $\frac{\sigma}{E_0}$, along the wall for the Froude number $Fr_1 = 33$, small step $\chi \approx 0.13$ and convergence angle $\theta = 5.5^\circ$.

Figures 21 and 22 display the influence of the chute step size on the pressure distribution. Figure 21 shows that the mean pressure distribution for small steps is slightly more stretched than for large steps. This can be attributed to the increase in energy dissipation in a stepped spillway with larger steps, which, in turn, leads to a decrease in mean velocities in the upstream section. With the increase in step size, pressure variations are slightly larger in the upstream regions of the basin walls (Figure 22). This can be explained by the more pronounced turbulence and energy dissipation at the upstream section for larger steps. On the other hand, downstream regions of the walls show that an increase in step size leads to the faster attenuation of pressure fluctuations. This could be attributed to the lower inflow residual energy required to sustain velocity fluctuations (and, in turn, pressure fluctuations as well).

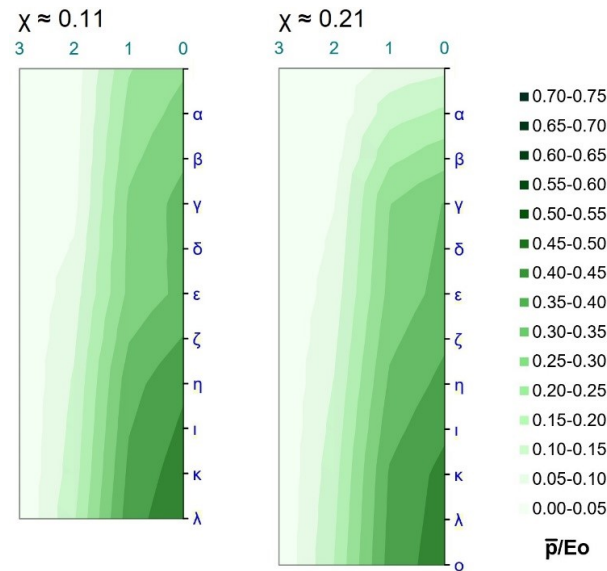


Figure 21. The influence of the chute step size, χ , on the mean pressures, $\frac{\bar{p}}{E_0}$, along the wall for the Froude number $Fr_1 = 30$, submergence ratio $\Omega = 1.04$ and convergence angle $\theta = 5.5^\circ$.

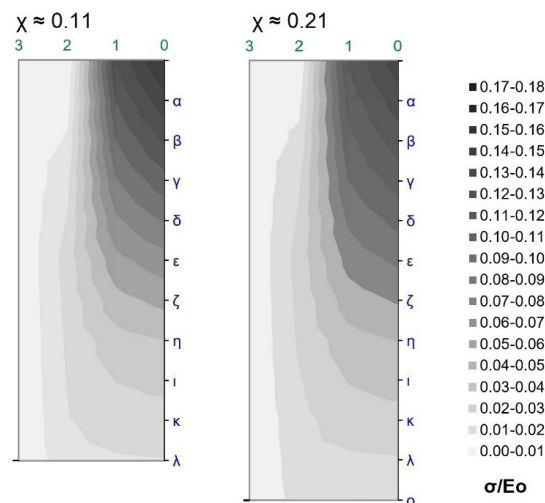


Figure 22. The influence of the chute step size, χ , on the pressure fluctuations, $\frac{\sigma}{E_0}$, along the wall for the Froude number $Fr_1 = 30$, submergence ratio $\Omega = 1.04$ and convergence angle $\theta = 5.5^\circ$.

3.3. Estimating Hydrodynamic Load

Due to the non-simultaneous occurrence of extreme pressures over the entire flow field (characteristic for the fluctuation loads), the procedure of direct statistical analysis (sorting of current values of total loads on the slab at the moment of sampling) for estimating the hydrodynamic loads was used. It is assumed that the probability density function of the sampled data can be well approximated by the normal distribution. With the adopted normal distribution, the maximum and minimum values of the fluctuation loads can be defined as:

$$Y'_{max} = -Y'_{min} = k \cdot \sqrt{Y'^2}, \tag{10}$$

where the load, Y , can be the vertical force, V , or a horizontal force, H , or the bending moment, M , and the coefficient k depends on the probability of occurrence, and for the probability of 99.9% equals 3.2.

For evaluation of the design hydrodynamic load (vertical force) at the bottom, V , the following regression expressions, based on the research presented in this paper, are proposed:

$$\bar{V}^* = \frac{\bar{V}}{W} = C_0 \cdot \left(1 + C_{\chi 0} \cdot \frac{\chi - \chi_0}{\chi_0}\right) \cdot (1 + C_{\theta 0} \cdot e^{-|\theta - \theta_0|}) \cdot \left(1 - \frac{2\chi - 3\chi_0}{\chi_0} \cdot C_{\chi \theta 0} \cdot e^{-|\theta - \theta_0|}\right) + (\Omega - \Omega_0) \cdot C_{\Omega} \cdot \left(1 + C_{\chi} \cdot \frac{\chi - \chi_0}{\chi_0}\right) \cdot \left(1 + C_{\theta} \cdot e^{-|\theta - \theta_0|} - \frac{m \cdot \theta^n}{2}\right) \quad (11)$$

$$V'^* = \frac{V'}{W} = K_0 \cdot \left(1 + K_{\chi 0} \cdot \frac{\chi - \chi_0}{\chi_0}\right) \cdot \left(1 + K_{\theta 01} \cdot \left(\frac{\theta}{\theta_0}\right)^2 + K_{\theta 02} \cdot e^{-\frac{|\theta - \theta_1|^4}{90}}\right) \cdot \left(1 + \frac{2\chi - 3\chi_0}{\chi_0} \cdot K_{\chi \theta 0} \cdot e^{-|\theta - \theta_0|}\right) + \frac{\Omega - \Omega_0}{\Omega^2} \cdot K_{\Omega} \cdot \left(1 + K_{\theta} \cdot e^{-|\theta - \theta_1|} - k \cdot e^{-\frac{|\theta - \theta_1|}{0.1}}\right) \quad (12)$$

where V^* is the dimensionless vertical force on the bottom slab from mean pressures, V'^* is the vertical dimensionless force from pressure fluctuations and W is the weight of the water above the stilling basin slab, as if the basin was completely filled with water at the tail-water level. Variable regression coefficients are presented in Tables 1 and 2 for Equations (11) and (12), respectively, and the constants are $\chi_0 = 0.127$, $\theta_0 = 5^\circ$ and $\Omega_0 = 1.112$.

Table 1. Regression coefficients for Equation (11) for the slab occupying: (a) entire bottom area, (b) upstream half of the bottom area, (c) downstream half of the bottom area.

	(a) Entire Slab	(b) Upstream Slab	(c) Downstream Slab
C_0	0.759	0.647	0.836
$C_{\chi 0}$	0.134	0.179	0.1
$C_{\theta 0}$	0.081	0.087	0.031
$C_{\chi \theta 0}$	-0.093	-0.013	-0.065
C_{Ω}	0.837	0.523	-0.347
C_{χ}	0.406	-0.167	0.929
C_{θ}	0.478	0.617	-0.179
m	-0.573	-0.092	-1.749
n	0.25	0.25	0.2

The mean deviations of the regression expressions from the measured values were 4.4%, 6.2% and 6.9% for the mean vertical force on the slab over the entire bottom, on the upstream half slab and on the downstream half slab, respectively.

The mean deviations for the fluctuation vertical force were 11.3%, 12.2% and 14.9% on the slab over the entire bottom, on the upstream half slab and on the downstream half slab, respectively.

Expressions (11) and (12) give reliable results within the domain $20 \leq Fr_1 \leq 70$; $0.1 \leq \chi \leq 0.3$; $0^\circ \leq \theta \leq 16.5^\circ$ and $1 \leq \Omega \leq 1.25$.

Design loads for the stilling-basin wall are the maximum horizontal force and the maximum bending moment. In all performed experiments, both loads had their maximum values at the very downstream end of the basin, where the water depth was equal to h_{TW} . These maximum loads occur as a cumulative effect of hydrostatic and hydrodynamic impacts. The experimental values of dimensionless mean horizontal force, $\bar{H}^* = \frac{H_m}{H_{TW}}$, and dimensionless mean moment, $\bar{M}^* = \frac{M_m}{M_{TW}}$, as hydrostatic components of maximum loads at the downstream end of the basin are shown in Figures 23 and 24, where H_{TW} and M_{TW} are the corresponding horizontal force and moment due to the hydrostatic pressure of the downstream water depth on the wall.

Table 2. Regression coefficients for Equation (12) for the slab occupying: (a) entire bottom area, (b) upstream half of the bottom area, (c) downstream half of the bottom area.

	(a) Entire Slab	(b) Upstream Slab	(c) Downstream Slab
K_0	0.07	0.115	0.059
$K_{\chi 0}$	-0.057	-0.098	-0.09
$K_{\theta 01}$	0	0	0.04
$K_{\theta 02}$	0.152	0.158	-0.158
$K_{\chi \theta 0}$	0.005	0.341	0.743
K_{Ω}	-0.105	-0.322	-0.045
K_{θ}	-0.513	0.437	-0.076
θ_1	9.007	9.434	5.33
k	-364.957	-162.869	-2.479

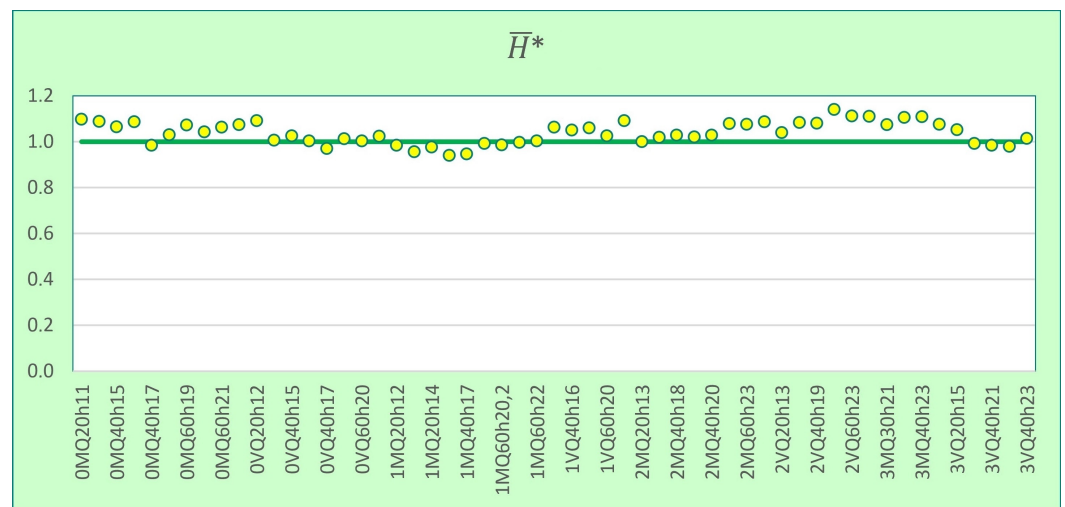


Figure 23. Experimental values of dimensionless mean horizontal forces. Circles represent dimensionless mean horizontal forces based on measures results, and the green line is proposed value of dimensionless mean horizontal force.

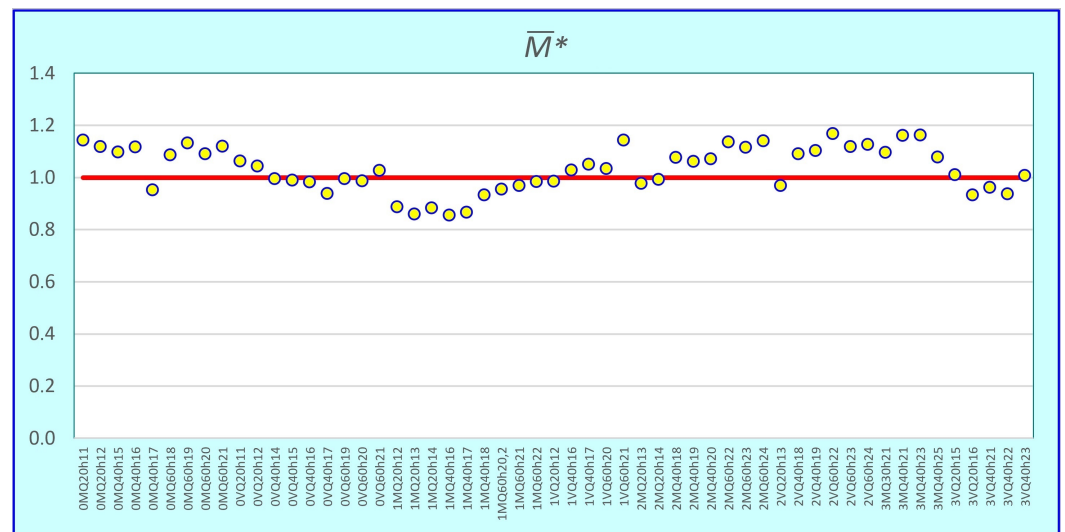


Figure 24. Experimental values of dimensionless mean bending moments. Circles represent dimensionless mean bending moments based on measures results, and the red line indicates the proposed value of dimensionless mean bending moment.

From Figures 23 and 24, it can be observed that the value of dimensionless loads is equal to unity, that is, the values of mean horizontal force and mean moment deviate very little from the corresponding static force and moment due to the downstream water depth. Therefore, the mean loads on the wall of the stilling basin can be calculated as:

$$\bar{H} = H_{TW}, \tag{13}$$

$$\bar{M} = M_{TW}. \tag{14}$$

The experimental values of dimensionless fluctuation horizontal force, $H'^* = \frac{H'}{H_{TW}}$, and dimensionless fluctuation moment, $M'^* = \frac{M'}{M_{TW}}$, at the downstream end of the basin are shown in Figures 25 and 26.

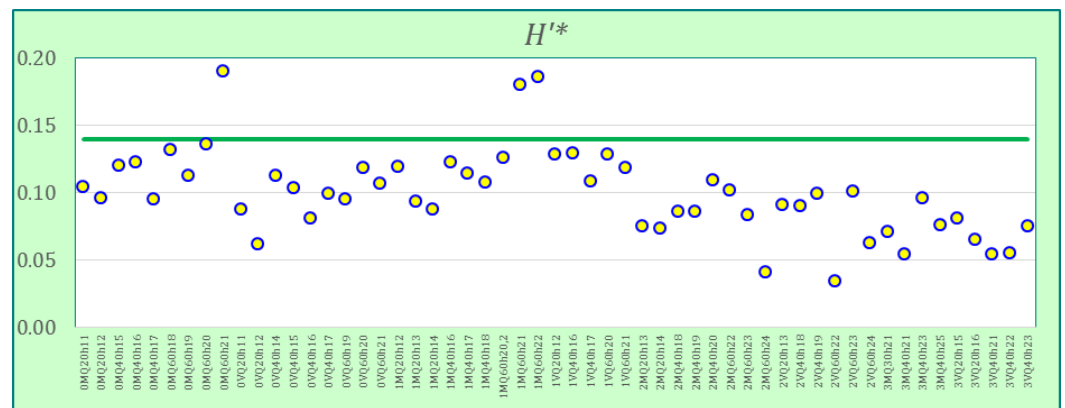


Figure 25. Experimental values of dimensionless fluctuation horizontal forces. Circles represent dimensionless fluctuation horizontal forces based on measures results, and the green line is proposed value of dimensionless fluctuation horizontal force.

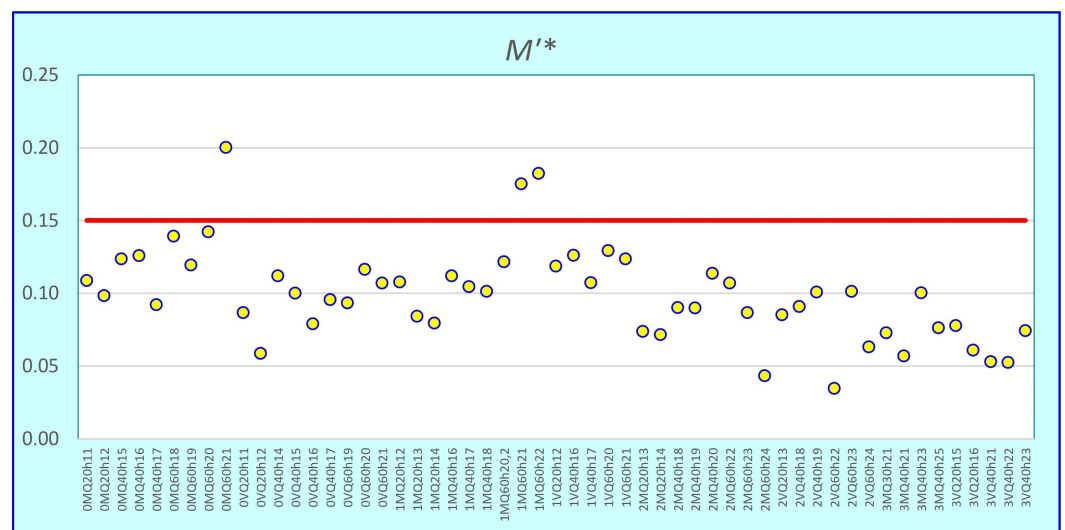


Figure 26. Experimental values of dimensionless fluctuation bending moments. Circles represent dimensionless fluctuation bending moments based on measures results, and the red line is proposed value of dimensionless fluctuation bending moment.

As seen from Figures 25 and 26, the values of fluctuating horizontal forces and moments commonly had a value between 5% and 15% of the corresponding hydrostatic

load from downstream depth. Fluctuation loads have extreme characteristics, so it is recommended that the envelopes of these loads be used for design:

$$H' = 0.14H_{TW}, \quad (15)$$

$$M' = 0.15M_{TW}. \quad (16)$$

4. Conclusions

In this paper, the results of the study of hydrodynamic loads (vertical force, horizontal force and bending moment) in a converging stepped-chute stilling basin are presented. This is the first study to address the dynamic loads of this type of structure and the first research concerning the loads on the stilling basin walls in general.

Pressure distribution in the stilling basin is influenced by the convergence angle of the walls of a spillway chute, inflow Froude number, submergence ratio and chute step size. Experimental results show that, in statistical sense, pressure distribution at every location can be well approximated with normal probability distribution.

The most influential appears to be the chute convergence angle. Its influence is mainly limited to the regions close to the upstream section of the basin.

Mean pressures (and forces) have the lowest values in the upstream parts of the basin and increase in the downstream direction, while pressure fluctuations have the largest impact in the upstream parts of the basin and diminish in the downstream direction.

From the measured pressure distributions, regression expressions for predicting hydrodynamic loads (vertical force for the bottom slabs and horizontal force and bending moment for the walls) are proposed. These expressions provide a reliable tool for the structural design of stepped-spillway stilling basins.

Practical limitations of the current research include a relatively narrow range of Froude numbers and convergence angles. Practically, further research should provide additional information, particularly for a larger range of Froude numbers. In addition, the study of other types of stilling basins (stilling basin with adverse slope bottom, stilling basin with diverging walls, etc.) and different types of energy dissipating devices (baffle blocks, dentated sill) could be performed.

Author Contributions: Conceptualization, V.K. and L.S.; Methodology, B.M. and P.V.; Software, B.M.; Validation, B.M., B.Z. and P.V.; Formal analysis, B.M. and L.S.; Investigation, B.M., B.Z. and P.V.; Resources, V.K. and L.S.; Data curation, L.S.; Writing—original draft preparation, B.M., B.Z. and L.S.; Writing—review and editing, B.M., B.Z., V.K. and L.S.; Visualization, B.M.; Supervision, V.K. and L.S.; Project administration, V.K. and L.S.; Funding acquisition, V.K. and L.S. All authors have read and agreed to the published version of the manuscript.

Funding: This research was funded by the Ministry of Education, Science and Technological Development of Serbia (grants TR37009 and TR37010).

Data Availability Statement: Measured and presented data are available upon request from the corresponding author.

Acknowledgments: Authors would like to acknowledge the help of Dragan Savic FREng for giving us valuable feedback during preparation of the manuscript.

Conflicts of Interest: The authors declare no conflict of interest.

References

1. Boes, R.M.; Hager, W.H. Hydraulic Design of Stepped Spillways. *J. Hydraul. Eng.* **2003**, *129*, 671–679. [[CrossRef](#)]
2. Chanson, H. *Hydraulics of Stepped Chutes and Spillways*, 1st ed.; Balkema: Lisse, The Netherlands, 2002; p. 424, ISBN 9789058093523.
3. Khatsuria, R.M. *Hydraulics of Spillways and Energy Dissipators*, 1st ed.; CRC Press: Boca Raton, FL, USA, 2004; p. 680, ISBN 9780824757892.
4. Ljubicic, R.; Zindovic, B.; Vojt, P.; Pavlovic, D.; Kapor, R.; Savic, L. Hydraulic Jumps in Adverse-Slope Stilling Basins for Stepped Spillways. *Water* **2018**, *10*, 460. [[CrossRef](#)]

5. Schleiss, A.J.; Ercicum, S.; Matos, J. Energy dissipation in stilling basins with side jets from highly convergent chutes. *Water* **2023**, *12*, 2161. [[CrossRef](#)]
6. Stojnic, I. Stilling Basin Performance Downstream of Stepped Spillways. Ph.D. Thesis, École Polytechnique Fédérale de Lausanne, Lausanne, Switzerland, 2020.
7. Ruff, J.F.; Ward, J.P. *Hydraulic Design of Stepped Spillways*; Report 99FC800156; U.S. Bureau of Reclamation: Denver, CO, USA, 2002; p. 245.
8. Zindovic, B.; Vojt, P.; Kapor, R.; Savic, L. Converging stepped spillway flow. *J. Hydraul. Res.* **2016**, *6*, 699–707. [[CrossRef](#)]
9. Moran, R.; Toledo, M.A.; Peraita, J.; Pellegrino, R. Energy dissipation in stilling basins with side jets from highly convergent chutes. *Water* **2021**, *13*, 1343. [[CrossRef](#)]
10. Morera, L.; San Mauro, J.; Salazar, F.; Toledo, M.Á. Highly-converging chutes as an overtopping protection for concrete dams: Physical and numerical modelling. In Proceedings of the 1st International Seminar on Dam Protections against Overtopping and Accidental Leakage, Madrid, Spain, 24–25 November 2014; pp. 245–257.
11. Toso, J.W.; Bowers, E. Extreme Pressures in Hydraulic-Jump Stilling Basins. *J. Hydraul. Eng.* **1988**, *8*, 829–843. [[CrossRef](#)]
12. Melo, J.F.; Pinheiro, A.N.; Ramos, C.M. Forces on plunge pool slabs: Influence of joints location and width. *J. Hydraul. Eng.* **2006**, *132*, 49–60. [[CrossRef](#)]
13. Peterka, A.J. *Hydraulic Design of Stilling Basins and Energy Dissipators*, 8th ed.; United States Bureau of Reclamation: Denver, CO, USA, 1984; p. 225.
14. Sánchez-Juny, M.; Dolz, J. Experimental study of transition and skimming flows on stepped spillways in RCC dams: Qualitative analysis and pressure measurements. *J. Hydraul. Res.* **2005**, *5*, 540–548. [[CrossRef](#)]
15. Bellin, A.; Fiorotto, V. Direct Dynamic Force Measurement on Slabs in Spillway Stilling Basins. *J. Hydraul. Eng.* **1995**, *10*, 686–693. [[CrossRef](#)]
16. Fiorotto, V.; Rinaldo, A. Turbulent pressure fluctuations under hydraulic jumps. *J. Hydraul. Res.* **1992**, *4*, 499–520. [[CrossRef](#)]
17. Farhoudi, J.; Narayanan, R. Force on Slab Beneath Hydraulic Jump. *J. Hydraul. Eng.* **1991**, *1*, 64–82. [[CrossRef](#)]
18. Hajdin, G. Estimate of the fluctuating load on solid surfaces based on the pressure measurements in a finite number of gauging points. In Proceedings of the Yugoslav Society of Hydraulic Engineers, Portoroz, Yugoslavia, 2–4 December 1982.
19. Vasiliev, O.F.; Bukreyev, V.I. Statistical Characteristics of Pressure Fluctuations in the Region of Hydraulic Jump. In Proceedings of the 12th IAHR Congress, Fort Collins, CO, USA, 11–14 September 1967.
20. Castillo, L.G.; Carrillo, J.M. Pressure and Velocity Distributions in Plunge Pools. In Proceedings of the 2nd International Seminar on Dam Protection against Overtopping, Fort Collins, CO, USA, 7–9 September 2016.
21. Stojnic, I.; Pfister, M.; Matos, J.; Schleiss, A.J. Plain Stilling Basin Performance below 30° and 50° Inclined Smooth and Stepped Chutes. *Water* **2022**, *14*, 3976. [[CrossRef](#)]
22. Valentin, G.; Volkart, P.U.; Minor, H.E. Energy dissipation along stepped spillways. In *Hydraulics of Dams and River Structures*; Yazdandoost, F., Attari, J., Eds.; Taylor & Francis: Boca Raton, FL, USA, 2004; pp. 273–278, ISBN 9789058096326.
23. Milovanovic, B. Hydrodynamic Loads on the Evacuation Facilities of Hydraulic Structures. Ph.D. Thesis, Faculty of Civil Engineering, University of Belgrade, Belgrade, Serbia, 2018.
24. Ljubicic, R.; Vicanovic, I.; Zindovic, B.; Kapor, R.; Savic, L. Image processing for hydraulic jump free-surface detection: Coupled gradient/machine learning model. *Meas. Sci. Technol.* **2020**, *31*, 104003. [[CrossRef](#)]
25. Novak, P.; Moffat, A.I.B.; Nalluri, C.; Narayanan, R. *Hydraulic Structures*, 4th ed.; Taylor & Francis: Abingdon, UK, 2006; p. 700, ISBN 9780415386265.
26. Amador, A.; Sánchez-Juny, M.; Dolz, J. Developing Flow Region and Pressure Fluctuations on Steeply Sloping Stepped Spillways. *J. Hydraul. Eng.* **2009**, *12*, 1092–1100. [[CrossRef](#)]

Disclaimer/Publisher’s Note: The statements, opinions and data contained in all publications are solely those of the individual author(s) and contributor(s) and not of MDPI and/or the editor(s). MDPI and/or the editor(s) disclaim responsibility for any injury to people or property resulting from any ideas, methods, instructions or products referred to in the content.